Thin Solid Films 608 (2016) 44–49

Contents lists available at ScienceDirect

Thin Solid Films

journal homepage: www.elsevier.com/locate/tsf

Electrical transport properties of $Ni_{80}Fe_{20}$/HCl-PANI composites

Shanshan Xu, Jiahuan Yan, Zhe Feng, Suiyu Qiu, Fuhui Shao, Mingxuan Li, Mingpeng Yu, Hong Qiu *

[a] Department of Physics, School of Mathematics and Physics, University of Science and Technology Beijing, 30 Xueyuanlu, Haidian District, Beijing 100083, China
[b] Beijing Engineering Technology Research Center of Detection and Application for Weak Magnetic Field, 30 Xueyuanlu, Haidian District, Beijing 100083, China

ARTICLE INFO

Article history:
Received 10 November 2015
Received in revised form 29 February 2016
Accepted 6 April 2016
Available online 9 April 2016

Keywords:
$Ni_{80}Fe_{20}$ film
HCl-doped polyaniline
Composite
Electrical transport property

ABSTRACT

$Ni_{80}Fe_{20}$ films with a thickness of 40–170 nm were sputter-deposited on HCl-doped polyaniline (HCl-PANI) substrates at 300 K, forming the $Ni_{80}Fe_{20}$/HCl-PANI composites. In order to study the electrical transport property of the composite, a temperature dependence of the resistance (R–T) within 2–290 K was measured from the film surface and from the substrate back surface, respectively. The R–T curve measured from the film surface is very different from that measured from the substrate back surface. With the increase of temperature, the former exhibits the transition from almost temperature-independent region to semiconducting region whereas the latter shows a decrease of resistance. The transition temperature increases with increasing film thickness. The composite shows the temperature-independent feature below the transition temperature and the semiconducting feature over the transition temperature. Furthermore, for the R–T curve measured from the substrate back surface, the resistance of the composite is smaller than that of the HCl-PANI. With the increase of film thickness, it decreases and trends to be stable. The interface layer between the film and the substrate plays an important role in the electrical property of the composite.

1. Introduction

The composites consisting of polymers and metal nanoparticles or metal films were widely studied because of their potential applications, e.g. references [1–10]. Recently, Ni and Au films were sputter-deposited on HCl-doped polyaniline (HCl-PANI) substrates at 300 K, forming Ni/HCl-PANI and Au/HCl-PANI composites. A temperature dependence of the resistance (R–T) within 5–300 K revealed that these composites exhibited the metal–semiconductor transition. The composite showed the metallic conduction feature below the transition temperature and the semiconducting feature over the transition temperature [11,12]. A two-resistor parallel model was used to explain the metal–semiconductor transition of Ni/HCl-PANI and Au/HCl-PANI composites [11–13]. This model could qualitatively but not quantitatively explain the R–T relationship of the composite. It is very important to further understand the mechanism of the R–T relationship. The present work will do further experiment to clarify the mechanism of the R–T relationship. In order to better understand the R–T relationship of the composite, the R–T curve was measured from the film surface and from the substrate back surface, respectively. Furthermore, except for the Ni film and the Au film, do the composites consisting of other metal films and HCl-PANI have the metal–semiconductor transition? Are their R–T relationships different from those of Ni/HCl-PANI and Au/HCl-PANI composites? The answers to these questions are valuable and significant for the fundamental viewpoint. On the other hand, $Ni_{80}Fe_{20}$ film has superior soft magnetic property and high anisotropic magnetoresistance. It can be used in magnetic read heads and in magnetic sensors [14–16]. Moreover, $Ni_{80}Fe_{20}$ is an alloy material and is different from Ni and Au. Thus, in the present work, $Ni_{80}Fe_{20}$ films are sputter-deposited on HCl-PANI substrates, forming the $Ni_{80}Fe_{20}$/HCl-PANI composites. Field emission scanning electron microscopy (FE-SEM) is used to observe the structure of the film. Atomic force microscopy (AFM) is used to observe the surface morphology of the HCl-PANI substrate. The R–T relationship of the composite is studied within 2–290 K as a function of the $Ni_{80}Fe_{20}$ film thickness.

2. Experimental procedure

All the chemical reagents were purchased from Beijing Chemical Works and were analytically grade. Only aniline was doubly distilled under reduced pressure and stored in refrigerator (at about 4 °C) prior to using. The other chemical reagents were used without further purification. HCl-PANI was chemically synthesized using the well-established polymerization procedure [17]. The polymerization procedure is summarized as follows: (1) Aniline (0.1 mol) was dissolved in 100 mL aqueous hydrochloric acid (HCl, 1 mol/L) taken in a three-neck flask. The mixture solution was cooled and stirred at −3 °C by a magnetic stirrer. (2) 51.5 mL ammonium persulfate solution (2.4 mol/L) in a constant pressure funnel was slowly added into the mixture solution for 1 h in order to avoid heating the reaction mixture. The reaction proceeded at −3 °C for 8 h. (3) The final solution was filtered. (4) The protonated precipitate was washed with deionized water, acetone and ethanol until the washing water, acetone and ethanol became colorless and

* Corresponding author.
E-mail address: qiuhong@sas.ustb.edu.cn (H. Qiu).

http://dx.doi.org/10.1016/j.tsf.2016.04.009
0040-6090/

the pH was equal to 7. (5) The powder was dried at 50 °C in oven for two days. The HCl-PANI powder was obtained.

The HCl-PANI powder was compacted to pellets with 0.32 mm in thickness and 15 mm in diameter. The HCl-PANI pellets were used as the substrates. The DC magnetron sputtering system (KYKY) with the target inclined to the substrate at an angle of 45° was used [18]. The HCl-PANI substrates were placed in the working chamber via a load-lock chamber, which prevents the working chamber from air during changing the sample. 40 nm-, 90 nm- and 170 nm-thick $Ni_{80}Fe_{20}$ films were sputter-deposited on the HCl-PANI substrates at 300 K, obtaining the $Ni_{80}Fe_{20}$/HCl-PANI composites. Prior to deposition, the working chamber was evacuated to a pressure lower than 2×10^{-4} Pa by using a turbo molecular pump. The Ar gas (99.9995% in purity) pressure was 2.0 Pa and the sputtering power applied to the $Ni_{80}Fe_{20}$ target (99.99% in purity) of 50 mm in diameter was fixed at 150 W. A distance between the target and the substrate was 100 mm. The substrate holder was rotated at a rotary rate of 8 rotation/min during deposition in order to obtain the uniformly thick film. The average deposition rate was 9 nm/min.

FE-SEM of SUPRA55 (Zeiss) was used to observe the crystalline structure of the $Ni_{80}Fe_{20}$ film. AFM of CSPM5000 (Ben Yuan Ltd.) was used to observe the surface morphology of the HCl-PANI substrate. A resistance of the $Ni_{80}Fe_{20}$/HCl-PANI composite was measured in the temperature range of 2–290 K using the Cryogen-Magnet system of CFM-5T-H3-CFVTI-1.6K-24.5 with the four-point probe (Cryogenic Inc.). The R–T curve was measured from the film surface and from the substrate back surface, respectively.

3. Results and discussion

Fig. 1 shows FE-SEM microphotographs of the 170 nm-thick $Ni_{80}Fe_{20}$ film sputter-deposited on the HCl-PANI substrate. As shown in Fig. 1, the film grows with thin columnar grains perpendicular to the substrate surface and many voids are formed at the grain boundaries, i.e., the film has a porous structure. The grain size is around 30 nm.

Fig. 2 shows R–T curves of the $Ni_{80}Fe_{20}$/HCl-PANI composites with different film thickness. The R–T curve was measured from the film surface. In Fig. 2, the resistance R at each temperature is normalized to the resistance R_2 at 2 K. As can be seen from Fig. 2, all the composites exhibit a transition from almost temperature-independent region to semiconducting region. The transition temperature increases with increasing film thickness. The composite shows the temperature-independent feature below the transition temperature and the semiconducting feature over the transition temperature. A temperature coefficient of resistance trends to zero with increasing film thickness in the almost temperature-independent region. A decrease of resistance with temperature becomes more marked with decreasing film thickness in the semiconducting region.

Fig. 3 shows R–T curves of the $Ni_{80}Fe_{20}$/HCl-PANI composites with different film thickness, plotted as lgR versus T. The R–T curve was measured from the substrate back surface. As a comparison, the R–T curve of the HCl-PANI substrate is also shown in Fig. 3. As can be seen from Fig. 3, the resistance of the composite decreases monotonously with increasing temperature, similarly to the HCl-PANI substrate. However, the change of composite resistance with temperature is not smooth compared with the HCl-PANI substrate. The resistance of the composite is smaller than that of the HCl-PANI substrate. The difference between the composite resistance and the substrate resistance becomes more marked with decreasing temperature. Moreover, as the film thickness increases, the resistance of the composite decreases and trends to be stable. The R–T curve measured from the film surface is different from that measured from the substrate back surface. In order to see clearly the difference between them, Fig. 4 shows the R–T curves measured from the film surface and from the substrate back surface. In Fig. 4, the resistance R at each temperature is normalized to the resistance R_{20} at 20 K. As can be seen from Fig. 4, the R–T curve measured from the film surface is very different from that measured from the substrate back surface. It means that the electrical transport property measured from the film surface is different from that measured from the substrate back surface.

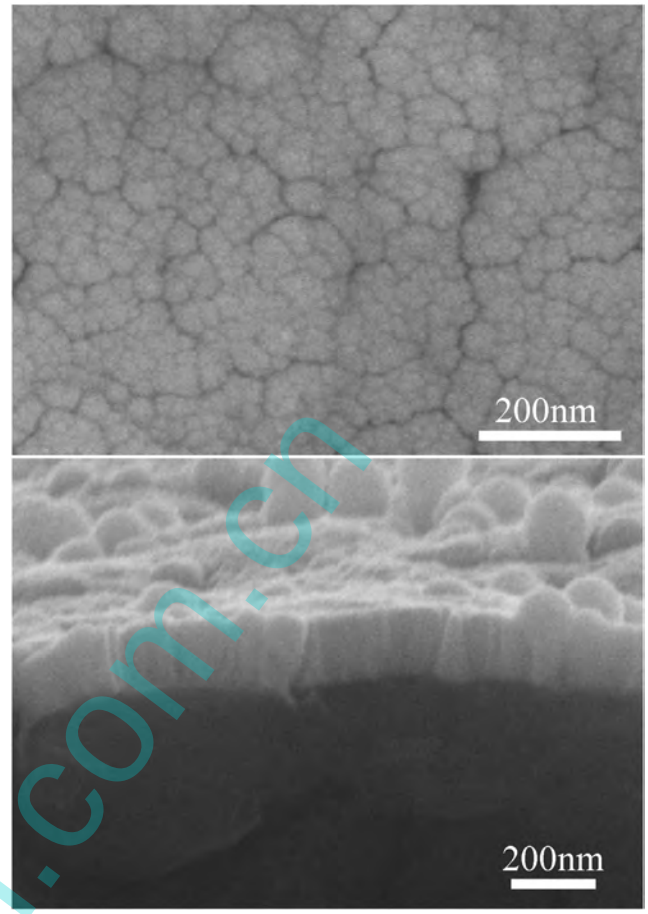

Fig. 1. FE-SEM microphotographs of the 170 nm-thick $Ni_{80}Fe_{20}$ film sputter-deposited on the HCl-PANI substrate.

In order to further understand the R–T relationship of the composite, the R–T curve of about 170 nm-thick $Ni_{80}Fe_{20}$ film sputter-deposited on SiO_2 at 300 K was measured in the temperature range of 3–300 K. Fig. 5 shows its R–T curve. In Fig. 5, the resistance R at each temperature is normalized to the resistance R_3 at 3 K. SiO_2 is a well-known insulator. Thus the measured R–T relationship comes from the $Ni_{80}Fe_{20}$ film. As

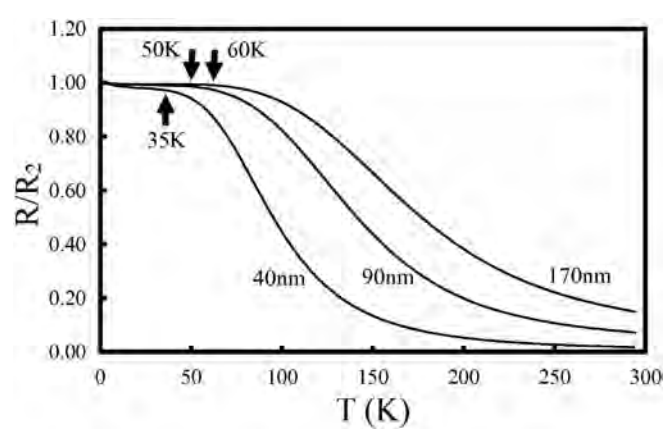

Fig. 2. R–T curves of the $Ni_{80}Fe_{20}$/HCl-PANI composites with different film thickness. The R–T curve was measured from the film surface. An arrow represents the transition temperature.

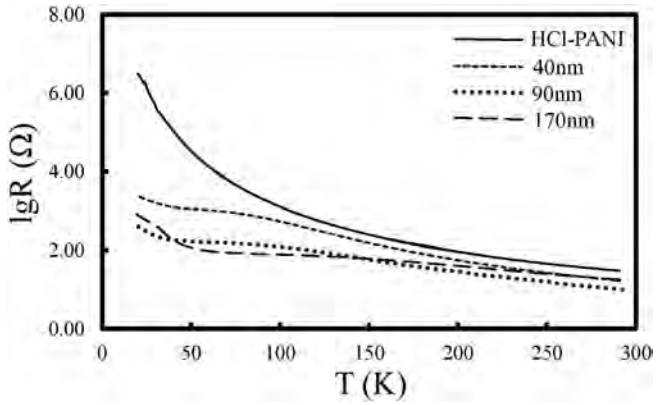

Fig. 3. R–T curves of the $Ni_{80}Fe_{20}$/HCl-PANI composites with different film thickness, plotted as lgR versus T. The R–T curve was measured from the substrate back surface.

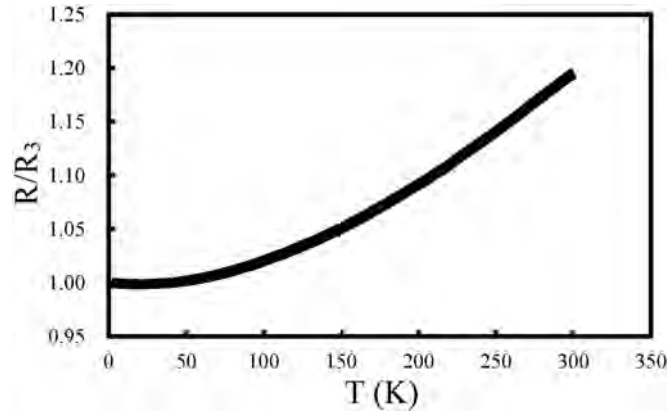

Fig. 5. R–T curve of the about 170 nm-thick $Ni_{80}Fe_{20}$ film sputter-deposited on SiO_2.

shown in Fig. 5, the R–T curve of the $Ni_{80}Fe_{20}$ film exhibits a metallic feature. It is different from the R–T curve of the $Ni_{80}Fe_{20}$/HCl-PANI composite.

Through the analysis of the results shown in Fig. 2, Fig. 3 and Fig. 5, the consideration is given as follows. When the resistance of the composite is measured from the film surface, the current flows into the $Ni_{80}Fe_{20}$ film and the HCl-PANI substrate. Thus the R–T curve shows the transition from almost temperature-independent region to semiconducting region. When the resistance of the composite is measured from the substrate back surface, the current only flows into the HCl-PANI substrate and does not flow into the $Ni_{80}Fe_{20}$ film. Thus the resistance decreases monotonously with increasing temperature. However, the R–T curve measured from the substrate back surface is different from that of the HCl-PANI substrate as shown in Fig. 3. Therefore, the electrical transport property measured from the substrate back surface is different from the electrical transport property of the HCl-PANI substrate. The R–T relationship of the HCl-PANI substrate can be explained by Mott three-dimensional (3D) variable range hopping (VRH) model [10,19,20]. In the 3D-VRH model, a temperature T dependence of conductivity σ can be expressed as [10,19,20]

$$\sigma = \sigma_0 \exp\left[-\left(\frac{T_0}{T}\right)^{\frac{1}{4}}\right] \quad (1)$$

where T_0 is the Mott characteristic temperature and σ_0 is the conductivity at $T = \infty$. T_0 and σ_0 are determined by the localization length, the density of state and the hopping distance in the material. Fig. 6 shows the σ–T relationship of the HCl-PANI substrate and a temperature dependence of conductance G in the $Ni_{80}Fe_{20}$/HCl-PANI composites, plotted as lnσ versus $T^{-1/4}$ and lnG versus $T^{-1/4}$. The conductance of the composite was measured from the substrate back surface. As can be seen from Fig. 6, the plot of the HCl-PANI substrate exhibits a good linear dependence having a linear correlation coefficient of 0.9995 whereas the plots of the composites show a nonlinear relationship. It means that the 3D-VRH model is suitable to explain the electrical transport property of the HCl-PANI substrate but unsuitable to explain that of the composite. Furthermore, it seems to indicate that the electrical transport property of the composite can be divided into three types in the high, middle and low temperature ranges, as shown in Fig. 6.

For the $Ni_{80}Fe_{20}$/HCl-PANI composites, in order to understand the R–T relationship measured from the substrate back surface, AFM was used to observe the surface morphology of the HCl-PANI substrate. Fig. 7 shows AFM image of the HCl-PANI substrate. A roughness of the substrate surface is about 18 nm. Thus it is considered that an interface layer is formed between the HCl-PANI substrate and the $Ni_{80}Fe_{20}$ film. The interface layer consists of HCl-PANI and $Ni_{80}Fe_{20}$ and its thickness is about 18 nm. The interface layer should influence the R–T curve of the $Ni_{80}Fe_{20}$/HCl-PANI composite. Fig. 8 shows a sketch of the R–T measurement in which the four-point probes are contacted on the substrate back surface. As shown in Fig. 8, the current is limited in the HCl-PANI substrate and the interface layer. Therefore, the R–T curve measured from the substrate back surface is determined by the R–T relationships of the substrate and the interface layer. As a result, the R–T curve

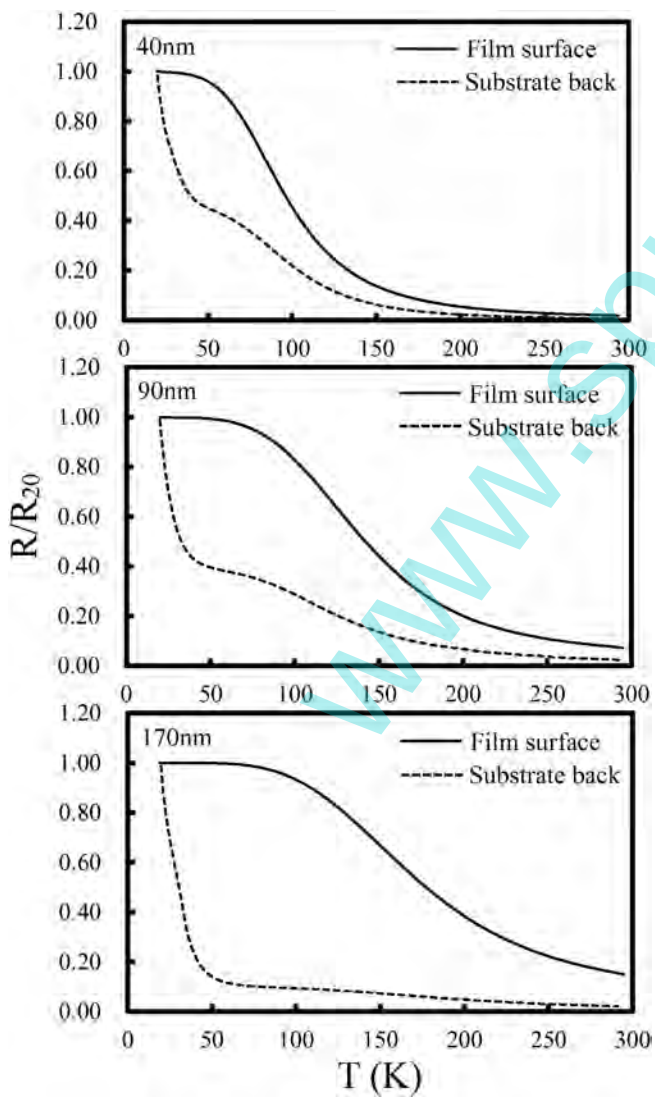

Fig. 4. R–T curves measured from the film surface and from the substrate back surface.

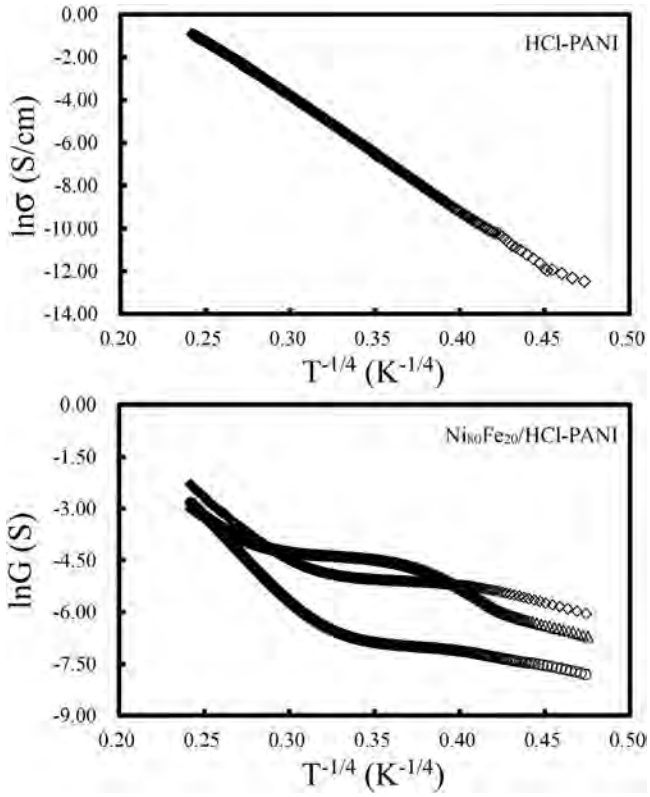

Fig. 6. σ–T relationship of the HCl-PANI substrate and temperature dependence of conductance G in $Ni_{80}Fe_{20}$/HCl-PANI composites, plotted as lnσ versus $T^{-1/4}$ and lnG versus $T^{-1/4}$. ○: 40 nm-thick film, : 90 nm-thick film, △: 170 nm-thick film.

measured from the substrate back surface is different from that of the substrate and that measured from the film surface.

When the R–T curve is measured from the substrate back surface, the measured composite conductance G (=1/R) is determined by the parallel of the substrate conductance G_s and the interface layer conductance G_i. Thus G_i can be expressed as

$$G_i = G - G_s \tag{2}$$

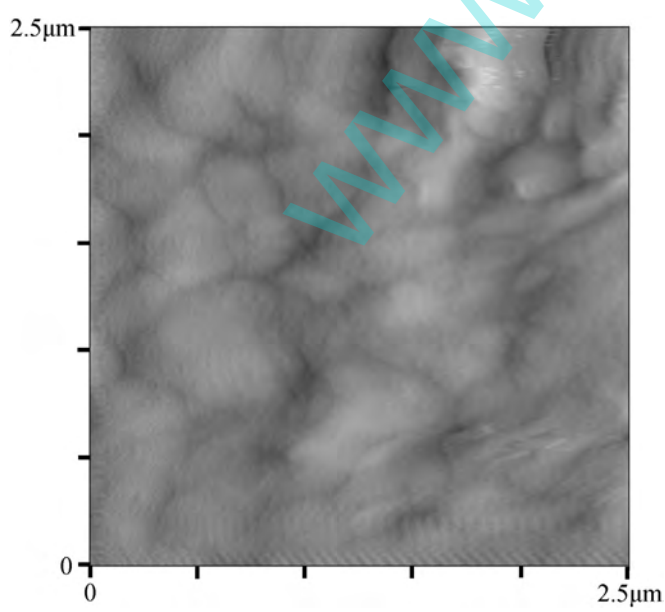

Fig. 7. AFM image of the HCl-PANI substrate.

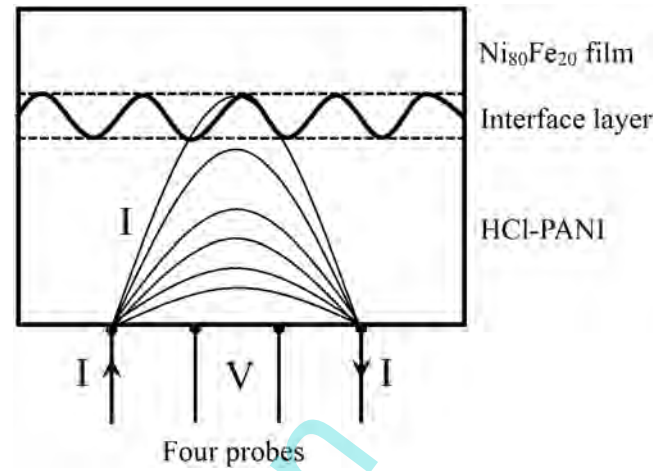

Fig. 8. Sketch of the R–T measurement in which the four-point probes are contacted on the substrate back surface.

where G is measured by the four-point probe technique and G_s is determined by the 3D-VRH model. Then, according to Eq. 2, the G_i–T curve of the interface layer can be obtained. Fig. 9 shows the G_i–T curves of the interface layers in the $Ni_{80}Fe_{20}$/HCl-PANI composites with different film thickness. As can be seen from Fig. 9, for all the composites, the conductance of the interface layer increases mainly with increasing temperature. The interface layer consists of HCl-PANI and $Ni_{80}Fe_{20}$. The 3D-VRH model and the thermally activated band conduction model are considered to explain the conductive mechanism in the interface layer. Using the 3D-VRH model, G_i is given by [10,19,20]

$$G_i = G_0 \exp\left[-\left(\frac{T_0}{T}\right)^{\frac{1}{4}}\right] \tag{3}$$

where G_0 is a constant. Fig. 10 shows the G_i–T curves of the interface layers in the $Ni_{80}Fe_{20}$/HCl-PANI composites with different film thickness, plotted as $\ln G_i$ versus $T^{-1/4}$. As shown in Fig. 10, the G_i–T relationship is nonlinear, indicating that the electrical transport property of the interface layer cannot be simply explained by the 3D-VRH model. According to the thermally activated band conduction model, G_i can be expressed as [21,22]

$$G_i = G_1 \exp\left(-\frac{\Delta E}{kT}\right) \tag{4}$$

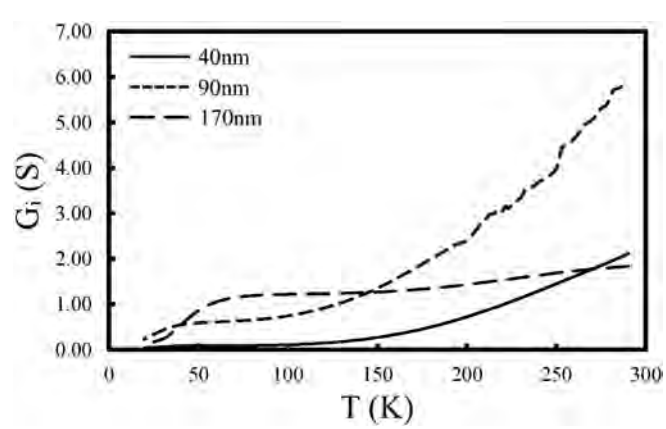

Fig. 9. G_i–T curves of the interface layers in the $Ni_{80}Fe_{20}$/HCl-PANI composites with different film thickness.

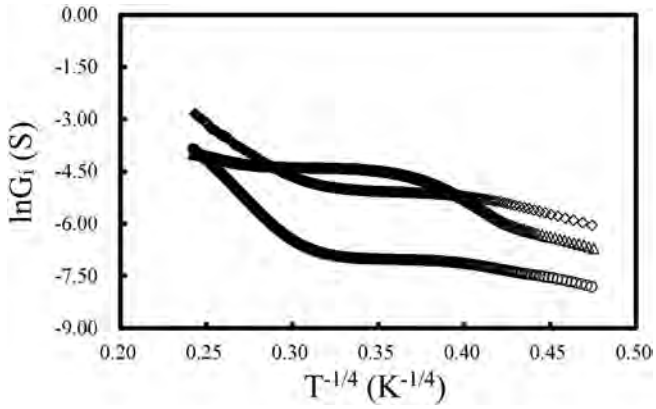

Fig. 10. G_i–T curves of the interface layers in the $Ni_{80}Fe_{20}$/HCl-PANI composites with different film thickness, plotted as $\ln G_i$ versus $T^{-1/4}$. ○: 40 nm-thick film, : 90 nm-thick film, △: 170 nm-thick film.

where G_1 is a constant, ΔE is the activation energy and k is the Boltzmann's constant. Fig. 11 shows the G_i–T curves of the interface layers in the $Ni_{80}Fe_{20}$/HCl-PANI composites with different film thickness, plotted as $\ln G_i$ versus T^{-1}. As can be seen from Fig. 11, the G_i–T relationship is also nonlinear, indicating that the electrical transport property of the interface layer cannot be simply explained by the thermally activated band conduction model. It is considered that the electrical transport property in the low temperature range is the 3D-VRH and that in the high temperature range is the thermally activated band conduction. Fig. 12 shows the G_i–T curves of the interface layers in the $Ni_{80}Fe_{20}$/HCl-PANI composites with different film thickness, plotted as $\ln G_i$ versus $T^{-1/4}$ below 40 K and $\ln G_i$ versus T^{-1} over 130 K. As shown in Fig.12, these plots exhibit a linear relationship having a linear correlation coefficient better than 0.98. Therefore, the electrical transport property in the low temperature range is the 3D-VRH and that in the high temperature range is the thermally activated band conduction. For the thermally activated band conduction mechanism, the activation energy is calculated in terms of the slop of the fitted straight line. The activation energy is 53 meV for the 40 nm-thick film, 35 meV for the 90 nm-thick film and 12 meV for the 170 nm-thick film.

According to the results mentioned above, the interface layer between the $Ni_{80}Fe_{20}$ film and the HCl-PANI substrate can play an important role in the electrical property of the $Ni_{80}Fe_{20}$/HCl-PANI composite. As a result, the three-resistor parallel model is suitable to explain the electrical transport property of the composite. Namely, the resistance of the composite can be calculated in terms of three parallel resistors,

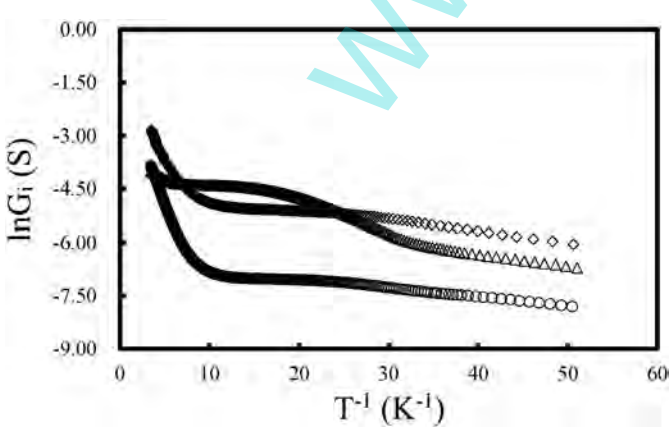

Fig. 11. G_i–T curves of the interface layers in the $Ni_{80}Fe_{20}$/HCl-PANI composites with different film thickness, plotted as $\ln G_i$ versus T^{-1}. ○: 40 nm-thick film, : 90 nm-thick film, △: 170 nm-thick film.

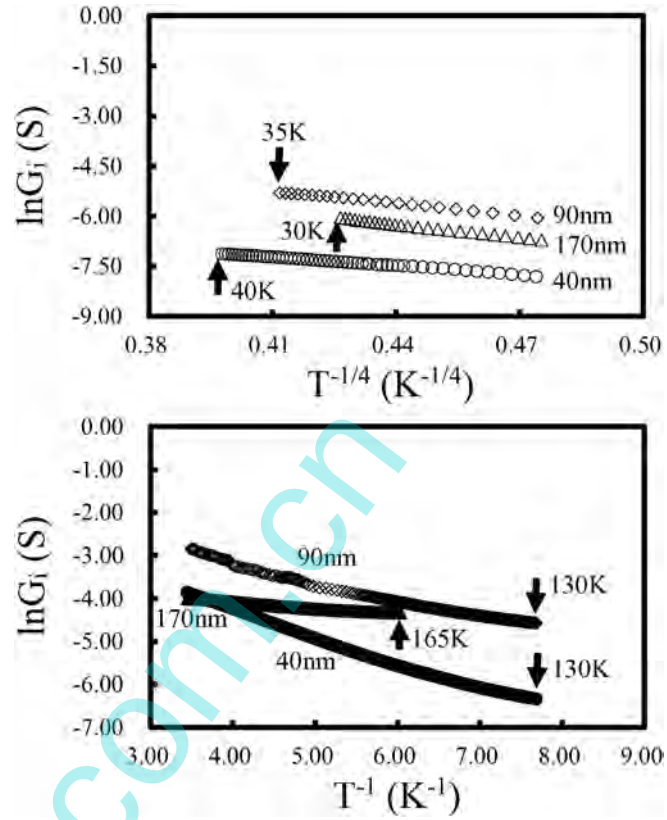

Fig. 12. G_i–T curves of the interface layers in the $Ni_{80}Fe_{20}$/HCl-PANI composites with different film thickness, plotted as $\ln G_i$ versus $T^{-1/4}$ below 40 K and $\ln G_i$ versus T^{-1} over 130 K.

i.e., the film resistance, the interface layer resistance and the substrate resistance. The existence of interface layer resistance leads to the difference between the experimental and theoretical results reported previously [11–13]. However, the structural and electrical properties of the interface layer is too complicated to be identified. Only when the structural and electrical properties of the interface layer is well identified, the R–T curve of the composite can be quantitatively explained by the three-resistor parallel model. The further study on the interface layer should be done. According to the difference between the R–T curves measured from the film surface and from the substrate back surface, it is possible to experimentally evidence the existence of the interface layer. It should be meaningful in practical applications.

4. Summary

The $Ni_{80}Fe_{20}$ films with a thickness of 40–170 nm were sputter-deposited on the HCl-PANI substrates at 300 K, forming the $Ni_{80}Fe_{20}$/HCl-PANI composites. The R–T curve measured from the film surface is very different from that measured from the substrate back surface. With the increase of temperature, the former exhibits the transition from almost temperature-independent region to semiconducting region whereas the latter shows a decrease of resistance. The transition temperature increases with increasing film thickness. The composite shows the temperature-independent feature below the transition temperature and the semiconducting feature over the transition temperature. Furthermore, for the R–T curve measured from the substrate back surface, the resistance of the composite is smaller than that of the HCl-PANI. With the increase of film thickness, it decreases and trends to be stable. The interface layer between the film and the substrate plays an important role in the electrical property of the composite.

Acknowledgment

The financial support from the Fundamental Research Funds for the Central Universities No. 8220 is gratefully acknowledged.

References

[1] F. Faupel, V. Zaporojtchenko, T. Strunskus, M. Elbahri, Metal-polymer nanocomposites for functional applications, Adv. Eng. Mater. 12 (2010) 1177–1190.
[2] F. Ruffino, V. Torrisi, G. Marletta, M.G. Grimaldi, Growth morphology of nanoscale sputter-deposited Au films on amorphous soft polymeric substrates, Appl. Phys. A Mater. Sci. Process. 103 (2011) 939–949.
[3] F. Ruffino, V. Torrisi, G. Marletta, M.G. Grimaldi, Effects of the embedding kinetics on the surface nano-morphology of nano-grained Au and Ag films on PS and PMMA layers annealed above the glass transition temperature, Appl. Phys. A Mater. Sci. Process. 107 (2012) 669–683.
[4] H. Takele, S. Jebril, T. Strunskus, V. Zaporojchenko, R. Adelung, F. Faupel, Tuning of electrical and structural properties of metal-polymer nanocomposite films prepared by co-evaporation technique, Appl. Phys. A Mater. Sci. Process. 92 (2008) 345–350.
[5] V. Torrisi, F. Ruffino, G. Isgro, I. Crupi, G.L. Destri, M.G. Grimaldi, G. Marletta, Polymer/metal hybrid multilayers modified Schottky devices, Appl. Phys. Lett. 103 (2013) 193117.
[6] F. Ruffino, V. Torrisi, G. Marletta, M.G. Grimaldi, Patterning of templated-confined nanoscale Au films by thermal-induced dewetting process of a poly(methylmethacrylate) underlying layer, J. Appl. Phys. 112 (2012) 124316.
[7] H. Takele, A. Kulkarni, S. Jebril, V.S.K. Chakravadhanula, C. Hanisch, T. Strunskus, V. Zaporojtchenko, F. Faupel, Plasmonic properties of vapour-deposited polymer composites containing Ag nanoparticles and their changes upon annealing, J. Phys. D. Appl. Phys. 41 (2008) 125409.
[8] T. Peter, M. Wegner, V. Zaporojtchenko, T. Strunskus, S. Bornholdt, H. Kersten, F. Faupel, Metal/polymer nanocomposite thin films prepared by plasma polymerization and high pressure magnetron sputtering, Surf. Coat. Technol. 205 (2011) S38–S41.
[9] Y. Cao, R.Y. Huang, B. Hu, H. Qiu, J.P. He, Structural and electrical properties of Ag films sputter-deposited on HCl-doped and undoped polyaniline substrates, Mater. Chem. Phys. 143 (2014) 788–793.
[10] R.C. Liu, H. Qiu, H. Li, H. Zong, C.Y. Fang, Fabrication and characteristics of composite containing HCl-doped polyaniline and Ni nanoparticles, Synth. Met. 160 (2010) 2404–2408.
[11] Z.W. Yang, H. Qiu, B. Hu, G.S. Zou, Structural and electrical properties of Ni films sputter-deposited on HCl-doped polyaniline substrates, Vacuum 99 (2014) 192–195.
[12] R.Y. Huang, Y. Cao, H. Qiu, Structural and electrical properties of Au films sputter-deposited on HCl-doped polyaniline substrates, Thin Solid Films 583 (2015) 158–162.
[13] S.Y. Qiu, Z.W. Yang, H. Qiu, Theoretical analysis on resistance-temperature characteristic of Ni/HCl-PANI composites, Adv. Mater. Res. 852 (2014) 142–146.
[14] M.P. Hollingworth, M.R.J. Gibbs, E.W. Hill, Surface, interface and bulk studies of NiFe nanometer films for magnetoresistive heads, J. Appl. Phys. 93 (2003) 8737–8739.
[15] P. Wu, F.P. Wang, H. Qiu, L.Q. Pan, Y. Tian, Effects of substrate temperature and annealing on the anisotropic magnetoresistive property of NiFe films, Rare Metals 22 (2003) 202–205.
[16] Y.T. Chen, J.Y. Tseng, T.S. Sheu, Y.C. Lin, S.H. Lin, Effect of grain size on magnetic properties and microstructure of $Ni_{80}Fe_{20}$ thin films, Thin Solid Films 544 (2013) 602–605.
[17] P.N. Adams, P.J. Laughlin, A.P. Monkman, A.M. Kenwright, Low temperature synthesis of high molecular weight polyaniline, Polymer 37 (1996) 3411–3417.
[18] M.P. Yu, H. Qiu, X.B. Chen, P. Wu, Y. Tian, Comparative study of the characteristics of Ni films deposited on SiO_2/Si(100) by oblique-angle sputtering and conventional sputtering, Thin Solid Films 516 (2008) 7903–7909.
[19] M. Gosh, A. Barman, A.K. Meikap, S.K. De, S. Chatterjee, Hopping transport in HCl doped conducting polyaniline, Phys. Lett. A 260 (1999) 138–148.
[20] J. Li, K. Fang, H. Qiu, S.P. Li, W.M. Mao, Micromorphology and electrical property of the HCl-doped and DBSA-doped polyanilines, Synth. Met. 142 (2004) 107–111.
[21] N. Serin, A. Yildiz, A.A. Alsaç, T. Serin, Estimation of compensation ratio by identifying the presence of different hopping conduction mechanisms in SnO_2 thin films, Thin Solid Films 519 (2011) 2302–2307.
[22] S. Ilican, Y. Caglar, M. Caglar, F. Yakuphanoglu, Electrical conductivity, optical and structural properties of indium-doped ZnO nanofiber thin film deposited by spray pyrolysis method, Phys. E. 35 (2006) 131–138.